Toward a 3D Arterial Tree Bifurcation Model for Intra-Cranial Aneurysm Detection and Segmentation

Florent Autrusseau, Rafic Nader, Anass Nouri, Vincent Allinec, Romain Bourcier

Toward a 3D Arterial Tree Bifurcation Model for Intra-Cranial Aneurysm Detection and Segmentation

Florent Autrusseau
LTeN, Polytech'Nantes (U6607), and
RMeS (U1229), Univ. of Nantes, France
Florent.Autrusseau@univ-nantes.fr

Rafic Nader
LTeN, Polytech'Nantes (U6607)
La Chantrerie 44306 Nantes, France
Rafic.Nader@univ-nantes.fr

Anass Nouri
SETIME Lab, Faculty of Sciences,
Ibn Tofail Univ., 14000 Kenitra, Morocco
Anass.Nouri@uit.ac.ma

Vincent L'Allinec
CHU d'Angers
4 rue larrey, 49933 Angers
Vincent.Lallinec@chu-angers.fr

Romain Bourcier
INSERM, U1087, ITX, CHU de Nantes
8 Quai Moncousu, 44007 Nantes
Romain.Bourcier@univ-nantes.fr

***Abstract*—An accurate detection of intracranial aneurysms is of paramount importance for a timely diagnosis and a possible treatment. Indeed, intracranial aneurysms (ICA) need to be detected at an early stage, and their evolution must be closely monitored before any treatment becomes hazardous. Numerous methods have been proposed to detect ICA either on Digital Subtraction Angiography (DSA) on Computed Tomography Angiography (CTA), or Magnetic Resonance Angiography (MRA) Time-Of-Flight (TOF) modalities. In the present study, we are particularly interested in the saccular ICA occurring onto the vascular tree's bifurcations, and we specifically focus our research on MRA-TOF acquisitions. We propose a synthetic model of both the artery bifurcation and the aneurysm itself. We are able to very accurately model some vasculature bifurcations as they are represented on TOF acquisitions. Their geometrical disposition, the various background noises and the aneurysm's shapes and positions are rigorously reproduced. The purpose of this approach is to alleviate the burden of a ground-truth manual segmentation commonly required when using deep-learning for object detection or semantic segmentation. Our model is highly configurable and intends to produce vast datasets used to feed a Convolutional Neural Network (CNN) for the automatic detection and segmentation of the saccular ICAs. In this preliminary study we only intend to propose a model for 3D aneurysm-bearing bifurcations. Evidently, a thorough evaluation of the model's accuracy is conducted. A preliminary experiment was conducted on a reduced dataset in order to assess the applicability of our bifurcation model. In future works, we will enhance the bifurcation model and propose an in-depth evaluation via Deep Learning methods.**

***Index Terms*—intracranial aneurysm detection, synthetic bifurcation model**

I. Introduction

Intra-Cranial Aneurysms (ICA) are arterial hernias forming onto the brain vasculature. The formation of the aneurysm is painless, the patient has no way of suspecting the presence of an ICA on its vascular tree. The aneurysm itself does not cause any symptoms whatsoever, nevertheless, it is crucial to detect and monitor the said aneurysms, indeed the risk comes when an ICA ruptures. Effectively, the consequences of the rupture are devastating, it causes bleeding around the brain (subarachnoid hemorrhagic stroke). A ruptured aneurysm is life threatening, and if not causing immediate death, it can provoke some serious brain damage. Mortality rate due to a ruptured aneurysm has been estimated as high as 65%. Moreover, in case of a patient survival, a loss of various brain functions can result from the induced subarachnoid hemorrhage [1]. Thus, it is crucial to efficiently detect and monitor the ICA. The preferred imaging modalities used to inspect the vascular tree in search for ICA are the Digital Subtraction Angiography (DSA) or Time-Of-Flight (TOF) Magnetic Resonance Angiography (MRA). DSA provides a very high-quality representation of the vascular tree, and hence of the eventual aneurysms it may hold [2]. However, the DSA implies the injection of contrast liquid within the blood system and is an invasive imaging. DSA acquisitions benefit from a much better resolution, at the expense of the contrast liquid injection, and moreover, such imagery only displays a single hemisphere of the brain. The vascular tree can very easily be extracted from the DSA volume, as the background noise is significantly weaker than the contrast liquid being imaged. Contrary to the DSA, the MRA-TOF acquisitions are much noisier; apart from the vascular tree, various matters appear on the image: the grey/white matter, the Cerebro-Spinal Fluid (CSF), the ventricle, the corpus callosum, all such portions of the brain exhibit varying radio-opacities, and hence a different grey level onto the resulting acquired volume. Both a DSA and a TOF segmentation are shown on Fig 1; an aneurysm can be observed on each of these acquisitions.

Although the ICA can easily be spotted on the 3D binary segmentations (see inside the red circles), it is a much more tedious and complex task on the original acquisitions. Fig. 1 (bottom row) represents a single slice of the DSA and TOF acquisitions, again the aneurysms are circled in red. Browsing through an entire 3D MRI volume in search for an aneurysm (which sometimes can be rather small) is time consuming and tedious. Of course, one might consider making a diagnosis on the segmented volume, which would be much faster, but unfortunately, although some recent progress on image segmentation (especially thanks to deep learning approaches)

leads to better segmentation performances, there is still ample room for improvements. One cannot always fully trust the resulting segmented images, especially when the ICA can occur in hyposignal (e.g. -partially- treated aneurysms for instance). In this work, we are only interested in Unruptured ICAs (UIAs).

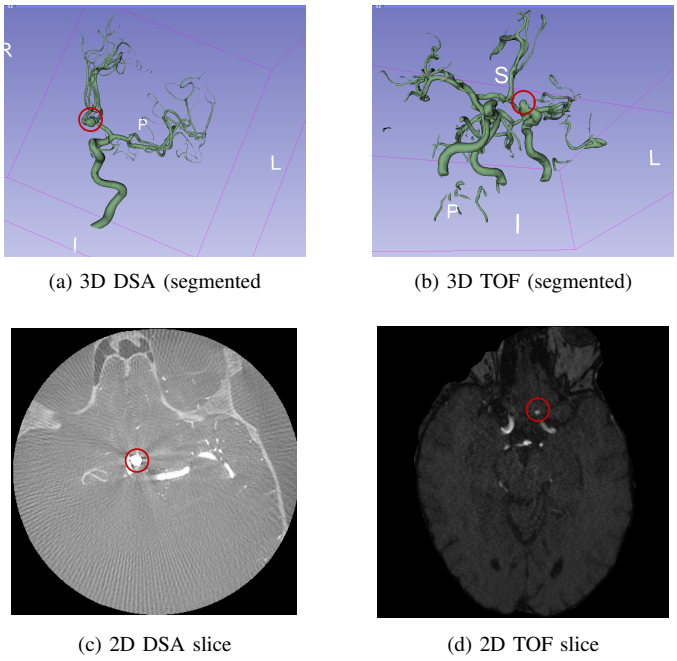

(a) 3D DSA (segmented

(b) 3D TOF (segmented)

(c) 2D DSA slice

(d) 2D TOF slice

Fig. 1. 3D segmented stacks, along with a example of 2D slice for DSA (left) and TOF (right) acquisitions.

ICA can present themselves in two different shapes, the fusiform aneurysms are identified by a local swelling of the artery, whereas the saccular aneurysm (also known as berry aneurysms) forms a spherical protrusion. This latter form is predominant in the brain vascular tree, they represent up to 90% of all brain aneurysms. Moreover, such ICA most commonly occur on a specific structure of the vasculature named the "Circle of Willis" [3], [4]. Some studies claim that about 85% of the ICAs occur along this particular pattern of the vascular tree [5]. Moreover, the saccular aneurysms most often arise onto a bifurcation of the arterial tree. Indeed, the fluid motion within the arteries presses the blood against the arterial wall, which, if weakened (by a genetic predisposition, or various environmental factors), will entail the aneurysm formation.

The efficient detection and segmentation of unruptured intracranial aneurysms is a matter of great concern, many studies have been devoted to this task throughout the last few decades. The vast majority of the researches being conducted on ICA detection focus on DSA images [6], [7], fewer works have been devoted to MRA-TOF acquisitions. Furthermore, although ICA detection is a widely studied field [8], the aneurysm segmentation is more marginally investigated [9], [10]. Authors in [11] used a Bayesian optimized filter for the automatic detection of ICA on DSA acquisitions. Quite often, the authors turn to 2D projected images [8], such as Maximum Intensity Projection (MIP) for various tasks of pattern recognition, as such 2D projections offers a better contrast. In [12] a two-stage CNN architecture was used to detect intracranial aneurysms on 2D-DSA images. Deep Learning methods have been employed for aneurysm detection as well. Works in [13] for instance intended to detect ICAs within MRA-TOF using a CNN. The authors exploited 85 datasets of patients, which represented a total of 115 intracranial aneurysms. They relied on manual annotations of this whole dataset to train their system. It is stated in the paper that 60 examinations were performed on a 3T Siemens scanner, while 12 were performed on a 1.5T Siemens scanner. Similarly, in [14], works have been conducted to detect and segment intracranial aneurysms on CT-Angiography, but the aneurysms were to be found in the particular context of aneurysmal subarachnoid hemorrhage, which means that the rupture already took place. However, again, manual segmentations were conducted by neurosurgeons and radiologists on a large panel of patients (68 for training and 185 for the evaluation step). As far as Deep Learning is concerned, manual labeling is most often unavoidable. This indeed, is the problem we expect to tackle using our approach. Effectively the manual annotation of 3D volumes is a rather tedious task, and moreover, if this dataset was constituted of one single acquisition source (e.g. one MRI scanner from a given University hospital), then, the trained neural network might end up being inefficient on different acquisitions (different magnetic field strength, implying a different resolution, background noise or contrast). A challenge has very recently been organized in order to compare some state-of-the-art methods from the literature [10]. A training set was composed of 113 cases, whereas a test set was made of 141 cases, holding respectively 129 and 153 unruptured ICA. Both detection and segmentation tasks were targeted. The authors conclude that "*Methods for UIA detection and segmentation are encouraging but require further development before being able to be accurately used to detect, segment and quantify UIAs automatically*". We believe that, by providing huge image datasets, it might be possible to increase the detection and segmentation performances. If the CNN could learn on thousands or even tens of thousands of 3D volumes instead of only a few hundreds, significant improvements might be achieved.

The saccular bifurcation aneurysms being predominant onto the cerebral arterial tree, and more particularly onto the tree's bifurcations, this work focuses on this particular disposition. In this study, we aim to propose some means to automatically detect and segment the unruptured saccular intracranial aneurysms on MRA-TOF acquisitions. We propose to build up a full model of both the 3D bifurcation and the aneurysm, in order to train a deep learning network to recognize the ICA. Our approach here is somewhat similar to a previous project we have recently been investigating [15]. Nevertheless, the approach presented here is much more advanced, with regard to several aspects: *i)* in [15], a 2D artery dataset was built, whereas here, we aim to tackle not only the artery, but

rather the whole bifurcation in 3D; *ii)* the bifurcation bears an unruptured aneurysm; and *iii)*, the background noise is now characterized and modeled with a much better accuracy. However, it is important to notice that this current work is only devoted to the design of the model itself. We hereby aim to build up the 3D bifurcation along with it's associated aneurysm and also intend to fully evaluate the verisimilitude of the modeled bifurcation (and ICA). Future works will consider adopting Deep Learning for the detection and segmentation tasks. To the best of our knowledge, we propose the very first approach considering the implementation of a full numerical bifurcation model for ICA deep-learning segmentation.

This paper is structured as follows. In section II, we will present both the geometrical model (*i.e.* the topological layout of the arteries, the dark and the bright background areas) and the noise model being employed to generate a background noise being as realistic as possible. Section III is devoted to the presentation of our experimental results. We will first describe how some statistical properties are collected onto human MRI images to be later applied in our model. We provide some examples of the 3D bifurcation model, but most importantly, we show how the 3D U-Net can cope with the segmentation task. We conclude this work in section IV

II. Method

In order to properly feed a neural network, so that it can recognize and locate intracranial aneurysms, we aim to accurately model some three-dimension bifurcations as well as the ICA to be precisely embedded onto the bifurcation. The model will thus need to be composed of three distinct steps, first, the geometry of the three artery branches needs to be built, then, an artificial ICA is generated and fused with the bifurcation and finally, the surrounding noise will also have to be accurately modeled and combined with the synthetic bifurcation.

A. Geometrical model

1) Artery bifurcation: The composition of the 3D bifurcation is quite straightforward. We build a $60 \times 60 \times 60$ voxels cube, in which we randomly determine 3 points located onto the faces of the cube. We then build three linear segments passing through these 3 points and grouping at the centroid of the cube. This basically forms the skeleton of the bifurcation. The next step consists of bringing some thickness to the three branches. We thus simply convolve the so-obtained 3D skeleton with a binary sphere (of a variable radius). This produces a 3D bifurcation made of three thick linear branches. To make the model more realistic, we need to bring some geometric transformations onto the synthetic arteries. An elastic deformation[1] is thus applied [16], [17] onto the model, so as to mimic the tortuosity of real-life arteries.

2) Aneurysm model: The synthetic aneurysm is also simply modeled by composing a binary sphere that will be merged onto the binary bifurcation. The ICA will also endure geometric deformations, as in human brains, the ICA commonly exhibit higher level distortions [18], [19]. As for the spatial positioning of the ICA, we seek to place the ICA approximately onto the angle bisector. Thanks to a 3D graph extraction from the vasculature skeleton [20], we can collect the 3D directional vectors initiated at the bifurcation center and following each of the three arteries (bifurcations' branches).

Let us denote $\vec{V_1}$, $\vec{V_2}$ and $\vec{V_3}$ the three vectors initiated at a bifurcation center (3D graph node) and tangent to the 3 branches centerlines. If we intend to embed an aneurysm in between branches 1 and 2, we must consider that the blood shall flow from branch 3 (mother branch). Indeed saccular ICA typically occur on the arterial wall opposite to the mother branch, as the blood pressure will be more important on this portion of the bifurcation. $\vec{V_1} + \vec{V_2}$ being the bisector line for this angle, we want the aneurysm to have a better alignment with branch 3. We thus plan to position the ICA as much as possible on the axis of the mother branch, and hence we compute the orientation that is along the orientation $\vec{V_0} = \vec{V_1} + \vec{V_2} - 2 \times \vec{V_3}$. Once this orientation determined, the distance of the aneurysm along this line must be estimated. We determine the distance $\mathcal{D}$ separating the bifurcation center to the aneurysm center (along $\vec{V_0}$) as shown on Eq. 1.

$$\mathcal{D} = \left(\frac{\overline{T}}{2} + r\right) \times \left(2 - \frac{\theta_{12}}{\pi \times (1 - 1/36)}\right), \qquad (1)$$

where θ_{12} is the angle formed by the branches #1 and #2, $\overline{T}$ is the average thickness of the 3 branches and r the aneurysm's radius. We consider that the angles cannot be smaller than 5° ($\pi/36\, rad$). This way, the smaller is the angle between the two branches, the further away will the ICA be embedded. On the opposite, for the largest angle configuration (180°), the ICA is approximately placed at $(\overline{T}/2 + r)$ voxels from the bifurcation center, i.e. the aneurysm is tangent to the bifurcation wall.

3) Modeling various radio-opacites: As previously explained, within a MRA-TOF acquisition, several matters appear on the brain image (the grey/white matter, the Cerebro-Spinal Fluid, the ventricle, the corpus callosum, etc.). We thus have to model these different areas, of varying radio-opacities. Commonly the arteries are surrounded by the brain fluids and are not directly located within the grey matter. It is thus important to encircle the bifurcations by the darkest background noise. In order to tackle this issue, we generate a distorted version of the segmented artery (binary shape) that will be used as a mask to arrange the darker area within the image. Applying elastic distortions to the artery mask will thus generate a new mask dedicated to the dark background noise.

B. Noise model

Noise in Magnetic Resonance Images (MRI) can be approximated by a Gaussian distributed noise [21]. Not only must we properly model the basic statistical properties of the target MRA-TOF (average and variance of the noise) but it is also critical to ensure that the spatial frequency of the modeled noise is a perfect match with the target MRI.

When going through Gaussian blur, the input image $I(x, y)$ is filtered as shown by eq. 2.

[1]The *ElasticDeform* library was used : https://elasticdeform.readthedocs.io/

$$O(x,y) = \sum_{i=-\infty}^{\infty} \sum_{j=-\infty}^{\infty} \frac{1}{2\pi\sigma_G^2} e^{-\frac{i^2+j^2}{2\sigma_G^2}} I(x+i, y+j) \quad (2)$$

The Bienaymé's identity states that

$$Var\left(\sum_{i=1}^{n} X_i\right) = \sum_{i=1}^{n} Var(X_i) + \sum_{i,j=1, i\neq j}^{n} Cov(X_i, X_j) \quad (3)$$

Thus, the variance of a linear combination is:

$$Var\left(\sum_{i=1}^{n} c_i X_i\right) = \sum_{i=1}^{n} c_i^2 Var(X_i) + 2 \times \sum_{i,j=1, i\neq j}^{n} c_i c_j Cov(X_i, X_j) \quad (4)$$

However, if $X_i, ..., X_n$ are pairwise independent integrable random variables ($Cov(X_i, X_j) = 0, \forall (i \neq j)$), which is our assumption in the following, then:

$$Var\left(\sum_{i} c_i X_i\right) = \sum_{i} c_i^2 Var(X_i) \quad (5)$$

where c_i are constants.

We consider that the variance of the input image is $Var\left[I(x+i, y+i)\right] = \sigma_0^2$, our goal here is to estimate the variance of the output (filtered) image $Var\left[O(x,y)\right] = \sigma_f^2$. Thus,

$$\sigma_f^2 = \sigma_0^2 \sum_{j=-\infty}^{\infty} \sum_{i=-\infty}^{\infty} \left(\frac{1}{2\pi\sigma_G^2} e^{-\frac{i^2+j^2}{2\sigma_G^2}}\right)^2 \quad (6)$$

For large σ_G, the squared Gaussian is smooth and the sum can be approximated as:

$$\sigma_f^2 \approx \sigma_0^2 \int_{-\infty}^{\infty} \int_{-\infty}^{\infty} \left(\frac{1}{2\pi\sigma_G^2} e^{-\frac{i^2+j^2}{2\sigma_G^2}}\right)^2 di.dj = \frac{\sigma_0^2}{4\pi\sigma_G^2} \quad (7)$$

and thus,

$$\sigma_f \approx \frac{\sigma_0}{2\sigma_G\sqrt{\pi}} \quad (8)$$

In summary, when an image composed of Gaussian noise of standard deviation σ_0 is being filtered by a Gaussian filter of standard deviation σ_G, the so-obtained filtered image has a standard deviation of σ_f according to the equation 8.

However, for our particular purpose, we intend to determine which Gaussian filter (of standard deviation σ_G) shall be used on the input image so as to obtain a filtered image with a given target statistics (σ_f), and hence $\sigma_G \approx \sigma_0/(2\sigma_f\sqrt{\pi})$.

The process starts thus with the generation of a high frequency Gaussian Noise of average set to our target 3D crop. This noise will then be filtered out using a Gaussian filter of standard deviation σ_G. The resulting image (of standard deviation σ_f) will thus present strong similarities with the target TOF.

III. Experimental results

This section is divided into three different parts. We first show how some statistical properties are collected onto target MRA-TOF acquisitions. In the second part, we provide some details on the dataset we have constituted. Finally, the third part is devoted to a full evaluation of the model with regards to different aspects (texture analysis and blur measure).

A. Statistical Modeling of the TOF volumes

In order to efficiently model the 3D bifurcations, and more specifically, the background noise, it is critical to gather some coherent statistics from the target MRI images. For this purpose, we have used Gaussian Mixture Models (GMM) to collect a range of target averages and standard deviations on 13 MRA-TOF volumes. Based on the assumption that a TOF volume contains 4 distinct components, which, ordered by increasing grey level would be: *i)* the black noisy background, *ii)* the various fluids, *iii)* the white/grey matter and *iv)* the arteries and possibly the fat tissues (if skull stripping methods were not applied). An example of a GMM fit with 4 components is shown on Fig. 2. The fourth component has been partially cut out of the plot, and is barely visible on this scale, as it accounts for the arteries, which represent very few pixels in this TOF slice (inset within the plot).

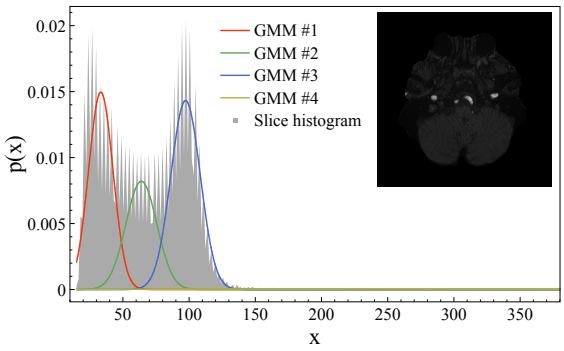

Fig. 2. One example of a fit with 4 components of a GMM.

The fat tissues, the meninges along with all unwanted portions or the MRI, such as the eyes, or nasal cavities can be discarded via the use of the Brain Extraction Tool (BET) [22], indeed, keeping these parts of the image might bias the results. We have thus applied BET prior to collect the statistics of the various background noises. The so-obtained skull-stripped images go through a GMM decomposition, see Eq. 9, where several Gaussian components $\mathcal{N}(\mu_i, \Sigma_i)$ are each weighted by an independent weight ϕ_i. This allows to gather the target averages and standard deviations of the various image portions we want to model. The collected averages and standard deviations can be observed on Fig. 3. In the following, the background noise representing the grey matter will be modeled according to the properties of the third Gaussian distribution. In this study, in order to limit the number of generated images, the voxel values for the darker portions of the image (ventricle, CSF) have simply be set to

two-thirds of the brighter noise. Future works will consider having a better differentiation between those two areas by considering both the second and third GMM.

$$p(x) = \sum_{i=1}^{N} \phi_i \mathcal{N}\left(x|\mu_i, \Sigma_i\right) \tag{9}$$

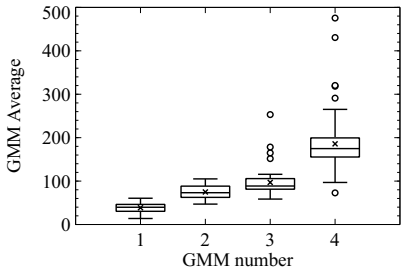

(a) Average

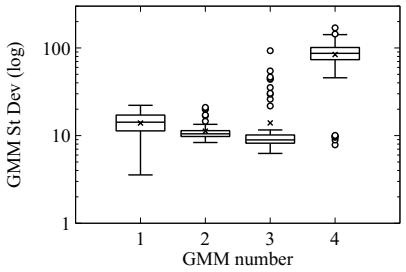

(b) Standard deviation

Fig. 3. Collected averages and standard deviations out of 13 MRA-TOF acquisitions (GMM with four components).

The bifurcation model can now be carried out using these statistical properties to modulate the synthetic noise that will be added up onto the modeled arteries.

B. Dataset constitution

Overall, the model was used to generate $5\,418$ bifurcations. For each bifurcation, when its configuration made it possible, we have independently embedded three ICA (one between each pair of branches). In total, $14\,073$ ICA were thus generated, with arteries diameters in the range $[4, 8]$, the amplitude (in grey levels) of the arteries were in $[220, 290]$, 3 different parameters were used for the elastic deformations, the target average of the background noise (white matter) was in the interval $[50, 110]$ whereas its standard deviation was in $[7, 11]$. As previously explained, the darker noise was simply set to $2/3$ of the white matter average. Four aneurysms' diameters have been modeled: 2, 4, 6 and 8 voxels (with two different distortion strengths). Table I encompasses the various geometrical and statistical settings being used by the model. During our experiments, we have witnessed a rather realistic rendering of the various matters composing the brain (*i.e.* CSF, grey/white matter, arteries, etc.) as shown on Fig. 4. Four different ICA are depicted on Figure 5, where we show some modeled 3D aneurysm-bearing bifurcations after a manual segmentation. This Figure shows how realistic is the positioning of the ICA onto the bifurcation. We did encounter a few cases where the aneurysm collar is slightly shifted away from the bifurcation center (see Fig. 5b and 5c for instance), but we believe that such a small shift might not influence much a CNN in its task of ICA detection and segmentation.

Vascular Property	Settings					
Artery Thickness	4	5	6	7	8	
Artery Amplitude	220	230	240	250	270	290
ElasticDeform (arteries)	3	4	5			
μ (background)	90	100	110			
σ_T (background)	7	9	11			
ElasticDeform (ICA)	2	3				
$\varnothing$ (ICA diam)	2	4	6	8		

TABLE I
VARIOUS PARAMETERS BEING USED BY THE MODEL.

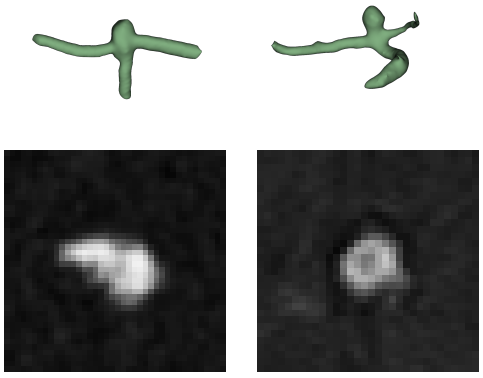

Fig. 4. A modeled (left column) and a true (right) ICA.

C. Evaluation of the bifurcation model

The very first purpose of our bifurcation model being to feed a CNN in order to automatically detect and segments Intra-Cranial Aneurysms, we obviously need to ensure that the model efficiently simulates some true ICAs. The bifurcation model must thus present very strong similarities with the true bifurcations collected from MRA-TOF acquisitions.

In order to assess the verisimilitude of our model, or in other words, its resemblance with the ground-truth, we have constituted a substantial dataset. Out of the full bifurcation dataset, 100 modeled bifurcations were (randomly) extracted from the 14.073 samples and Template Matching [23] was used to find the best matches with the MRA-TOF images. A matching 3D normalized correlation is highly unlikely, as the geometry of the images is too complex to efficiently match, and hence, we ran numerous 2D correlations. From the 100 bifurcations models, 10 slices were extracted from each 3D stack, they were correlated (using Template Matching) with 430 slices extracted from each tested TOF volumes (along the *x*, *y* and *z* orientations). Three different TOF were used, making a total of 1.000 modeled slices correlated with 1.290 TOF slices. We have set a matching threshold based on the Normalized Correlation Coefficient (NCC), all patches with a peak correlation such as $NCC > 0.75$, have been retained as good matches. Overall, the Template Matching allowed to collect more than 50.000 correlated patches. The statistics of the TOFs

(a) (b) (c) (d)

Fig. 5. Some example of modeled ICAs in 3D (after segmentation from the grey-level produced 3D model).

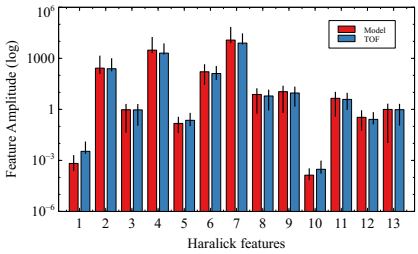

(a) Haralick features

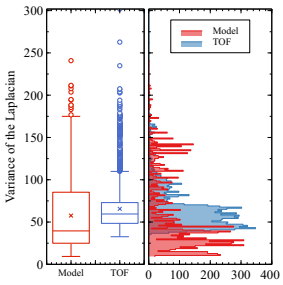

(b) Variance of Laplacian

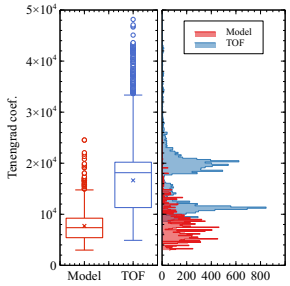

(c) Tenengrad coef.

Fig. 6. Evaluation of the model : (a) Haralick features, (b) Variance of the Laplacian and (c), Tenengrad coefficient.

are closely modeled, as previously shown in section II-B, but for a thorough analysis, we also ran a texture analysis and a blur factor evaluation. The Haralick features [24] were computed to ensure a good match of both textures (model and ground truth), as for the blur factor, both the Variance of the Laplacian and the Tenengrad coefficient [25] were computed. The Figure 6 shows a comparison between the model and three different TOF acquisitions with regard to these three measurements. The distribution of the data is displayed next to the box plot to show the (mis)matching dispersion. Although both the Haralick features and the Variance of the Laplacian seem to accurately match, the Tenengrad coefficient seems to drift a bit away in the Model. Hopefully, this drift might not be strong enough to have an impact on the upcoming use of this dataset for Deep Learning ICA detection.

In previous works [15], we managed to efficiently train a CNN (Half U-Net) using only modeled arteries, we believe that despite the more sophisticated model presented here (3D artery and ICA), such a training scenario should still be feasible. Moreover, the model might also be used as backup to some ground truth segmentations to train a neural network (acting as augmented data).

In order to evaluate the applicability of our model within a Deep Neural Network, we have set up a 3D U-Net to perform the segmentation of small 3D cropped bifurcations. The network was first trained on 120 modeled bifurcations and provided an average DICE score of 0.8 on a test set composed of 41 images, which is fairly close to the performances achieved in [15]. Next, to evaluate the model's suitability as a generator of augmented data, we have first launched the U-Net on 120 ground truth bifurcations, and then, on a set composed of both 40 ground truth and 80 modeled bifurcations. For both scenarios, the average DICE score was equivalent (≈ 0.94).

IV. Conclusion

In this work, we have presented a full 3D artery bifurcation model. More precisely, an aneurysm-bearing bifurcation model. Effectively, both the bifurcation and the aneurysm were built in such a way to best model the various features of MRA-TOF acquisitions. Evidently, the geometrical characteristics of the actual MRA bifurcations and ICA were respected. Moreover, the statistical properties of the background noise were collected from a set of target TOF images and accurately modeled. A thorough comparison between some ground-truth MRA volumes and the bifurcation+ICA model was conducted and showed that the resemblance might be sufficient for using a CNN in a ICA detection and segmentation task. Indeed, this work is a preliminary study on the feasibility of designing a fully synthetic artery bifurcation model. Using such a model to train a Deep Learning architecture can be very advantageous. Using such an approach, we avoid resorting to manual annotations on 3D volumes, which is a laborious task, and moreover, such manual annotations would have to be conducted on a very wide variety of MRI scanners for the Neural Network to apprehend the wide variety of image qualities. Using a model such as the one presented in this paper might help to train a CNN for a specific target MRI scanner. One single TOF acquisition is sufficient to gather some statistical properties and generate a vast image dataset that will be used to feed the network. A preliminary experiment was set up in order to evaluate the applicability of our model within a deep learning segmentation / recognition framework, this latter produced very encouraging results.

Acknowledgment

This work was partially supported by the French ANR-"WECAN" project.

REFERENCES

[1] R. A. Rava, S. E. Seymour, M. E. LaQue, B. A. Peterson, K. V. Snyder, M. Mokin, M. Waqas, Y. Hoi, J. M. Davies, E. I. Levy, A. H. Siddiqui, and C. N. Ionita, "Assessment of an artificial intelligence algorithm for detection of intracranial hemorrhage," World Neurosurgery, vol. 150, pp. e209–e217, 2021.

[2] A. Stafa and M. Leonardi, "Role of neuroradiology in evaluating cerebral aneurysms," Interventional Neuroradiology, vol. 14, pp. 23–37, 2008.

[3] H. Bogunovic, J. M. Pozo, R. Cardenes, L. S. Roman, and A. F. Frangi, "Anatomical labeling of the circle of willis using maximum a posteriori probability estimation," IEEE Transactions on Medical Imaging, vol. 32, no. 9, pp. 1587–1599, 2013.

[4] D. Robben, E. Türetken, S. Sunaert, V. Thijs, G. Wilms, P. Fua, F. Maes, and P. Suetens, "Simultaneous segmentation and anatomical labeling of the cerebral vasculature," Medical Image Analysis, vol. 32, pp. 201–215, 2016.

[5] A. Keedy, "An overview of intracranial aneurysms," McGill Journal of Medicine, vol. 9, no. 2, pp. 141–146, 2006.

[6] H. Jin, J. Geng, Y. Yin et al., "Fully automated intracranial aneurysm detection and segmentation from digital subtraction angiography series using an end-to-end spatiotemporal deep neural network," J Neurointerv Surg., vol. 12, no. 10, pp. 1023–1027, 2020.

[7] T. Jerman, F. Pernuš, B. Likar, and Z. Spiclin, "Computer-aided detection and quantification of intracranial aneurysms," in Medical Image Computing and Computer-Assisted Intervention (MICCAI), 10 2015, pp. 3–10.

[8] X. Dai, L. Huang, Y. Qian et al., "Deep learning for automated cerebral aneurysm detection on computed tomography images," Int J Comput Assist Radiol Surg., vol. 15, no. 4, pp. 715–723, 2020.

[9] D. Ueda, A. Yamamoto, M. Nishimori et al., "Deep learning for MR angiography: Automated detection of cerebral aneurysms," Radiology, vol. 290, no. 1, pp. 187–194, 2019, pMID: 30351253.

[10] K. Timmins, I. van der Schaaf, E. Bennink et al., "Comparing methods of detecting and segmenting unruptured intracranial aneurysms on TOF-MRAS: The ADAM challenge," NeuroImage, vol. 238, p. 118216, 2021.

[11] T. Hu, H. Yang, W. Ni, Y. Lei, Z. Jiang, K. Shi, J. Yu, Y. Gu, and Y. Wang, "Automatic detection of intracranial aneurysms in 3D-DSA based on a bayesian optimized filter," BioMedical Engineering OnLine, vol. 19, no. 1, p. 73, 2020.

[12] H. Duan, Y. Huang, L. Liu, H. Dai, L. Chen, and L. Zhou, "Automatic detection on intracranial aneurysm from digital subtraction angiography with cascade convolutional neural networks," BioMedical Engineering OnLine, vol. 18, no. 1, p. 110, 2019.

[13] T. Sichtermann, A. Faron, R. Sijben, N. Teichert, J. Freiherr, and M. Wiesmann, "Deep learning–based detection of intracranial aneurysms in 3D TOF-MRA," American Journal of Neuroradiology, vol. 40, no. 1, pp. 25–32, January 2019.

[14] R. Shahzad, L. Pennig, L. Goertz, F. Thiele, C. Kabbasch, M. Schlamann, B. Krischek, D. Maintz, M. Perkuhn, and J. Borggrefe, "Fully automated detection and segmentation of intracranial aneurysms in subarachnoid hemorrhage on CTA using deep learning," Scientific Reports, vol. 10, no. 1, p. 21799, 2020.

[15] S. Chater, N. Lauzeral, A. Nouri, Y. El Merabet, and F. Autrusseau, "Learning from mouse CT-scan brain images to detect MRA-TOF human vasculatures," in 43rd IEEE EMBC, 2021.

[16] O. Ronneberger, P. Fischer, and T. Brox, "U-Net: Convolutional networks for biomedical image segmentation," in Medical Image Computing and Computer-Assisted Intervention (MICCAI), ser. LNCS, vol. 9351. Springer, 2015, pp. 234–241.

[17] Özgün Çiçek, A. Abdulkadir, S. S. Lienkamp, T. Brox, and O. Ronneberger, "3D U-Net: Learning dense volumetric segmentation from sparse annotation," in Medical Image Computing and Computer-Assisted Intervention (MICCAI), vol. 2. Springer International Publishing, 2016.

[18] N. Juchler, S. Schilling, P. Bijlenga, D. Morel, S. Rüfenacht, V. Kurtcuoglu, and S. Hirsch, "Shape irregularity of the intracranial aneurysm lumen exhibits diagnostic value," Acta Neurochirurgica, vol. 162, pp. 2261–2270, 2020.

[19] N. Juchler, S. Schilling, S. Glüge, P. Bijlenga, D. R¨ ufenacht, V. Kurtcuoglu, and S. Hirsch, "Radiomics approach to quantify shape irregularity from crowd-based qualitative assessment of intracranial aneurysms," in 4th MICCAI workshop on Deep Learning in Medical Image Analysis, 2020, pp. 538–546.

[20] A. Nouri, F. Autrusseau, R. Bourcier, A. Gaignard, V. L'Allinec, C. Menguy, J. Veziers, H. Desal, G. Loirand, and R. Redon, "Characterization of 3D bifurcations in micro-scan and MRA-TOF images of cerebral vasculature for prediction of intra-cranial aneurysms," Elsevier Computerized Medical Imaging and Graphics, vol. 84C, 2020.

[21] A. Chaudhari and J. Kulkarni, "Noise estimation in single coil MR images," Biomedical Engineering Advances, vol. 2, p. 100017, 2021.

[22] S. Smith, "Fast robust automated brain extraction," Human Brain Mapping, vol. 17, no. 3, pp. 143–155, 2002.

[23] J. Lewis, "Fast normalized cross-correlation," in Vision interface, vol. 95, 1995.

[24] R. M. Haralick, "Statistical and structural approaches to texture," Proceedings of the IEEE, vol. 67, no. 5, pp. 786–804, 1979.

[25] U. Ali and M. Mahmood, "Analysis of blur measure operators for single image blur segmentation," Applied Sciences, vol. 8, no. 5, pp. 807–839, 2018.